Influence of γ-irradiation dose on the structure, linear and nonlinear optical properties of BiI₃ thick films for optoelectronics

A. M. Abdelnaeim[a], M. Salah[a], E. El Sayed Massoud[b,c], A. EL-Taher[a],
E. R. Shaaban[a,*]
aDepartment of Physics, Faculty of Science, Al-Azhar University, Assiut
bDepartment Biology, Faculty of Sciences and Arts in Dahran Aljanoub, King Khalid University, Saudi Arabia,
cAgriculture Research Center, Soil, Water and Environment Research Institute, Giza, Egypt

In this study, 900 nm of BiI₃ thick films were prepared using the thermal evaporation technique. There were exposed to different doses (0, 50, 100, 150, 200, 250, and 300 kG) of γ-radiation. The microstructure properties (Crystallite size and lattice strain) were calculated in terms of Scherrer's equation. With increasing γ-radiation doses, the Crystallite size increases, Both the refractive index and the film thicknesses have been calculated using Swanepoel's method. The optical band gap was measured in terms of transmittance and reflection spectrum in the high region of the absorption. The possible optical transition in the as-deposited and treated films are found to allow direct transition with energy gap increases with increasing γ-radiation doses. Dielectric constant, volume-energy-loss function (VELF), and surface-energy-loss function (SELF) for as-deposited films were discussed in terms of γ-radiation doses. The change in optical parameters has been interpreted in terms of the change in microstructure parameters. In terms of changes in energy gap and optical constants as a function of γ-radiation doses, BiI₃ thick films are recommended to use in optical devices and solar cells.

1. Introduction

BiI₃ has the space group R-3 and is a layered compound. That is, it possesses a rhombohedral/trigonal lattice with iodine atoms in the lattice points and bismuth cations filling two-thirds of the octahedral holes [1]. Because the trigonal crystal system is a member of the hexagonal crystal family, joining BiI₃ unit cells results in a hexagonal crystal system. A hexagonal structure is formed in three dimensions. layered semiconductor nanoparticles such as BiI₃, PbI₂, HgI, and MoS₂ are potential uses in photovoltaics, detectors, sensors, photocatalysis, lubrication, nonlinear optics, and photo-electrochemistry. They have benefits such as improved transport characteristics (inside a layer), fewer defects due to virtually perfect surfaces with almost no dangling bond perpendicular to the layer, and significant visual absorption due to tiny band gaps [2– 4]. Many works have been done on BiI₃ based on its structural [5], electronic [6, 7] and optical [8– 11] features. Krylova et al. [12], studied the absorption and luminescence spectra of BiI₃ crystals in a low-temperature range (1.6 – 77 K). H. Kondo et al[13] also investigated the luminescence characteristic of BiI₃. Thick films of BiI₃ have been studied for hard radiation detection and X-ray imaging because of the quite wide bandgap (1.67 eV)[14] and great mass density [15–17]. Also, BiI₃ has been utilized as a nanoscale pressure sensor[18] and a photodetector[19]. The current work reports the investigation of structural and optical features of BiI₃ nanocrystalline thick films with different thicknesses. Since the thermal evaporation technique is used to obtain different thicknesses of BiI₃ thick films. XRD is used to investigate the structural parameters of the studied thick films. The optical characterization is obtained using a double beam

UV/Vis Spectrophotometer. The film's thicknesses and subsequently the other optical constants are measured accurately according to the Swanepoel method.

The current work focuses on (1) using the Scherrer and Wilson equations to calculate structural parameters (crystallite size and lattice strain) of different doses (0, 50, 100, 150, 200, 250, and 300 kG) of γ-radiation, (2) using the developed envelope equations for maximum and minimum to calculate the refractive index, as suggested by Swanepoel, (3) calculating the dielectric constants, volume energy, surface energy, energy gap and nonlinear refractive index for photovoltaic and nonlinear optics and (4) interpreting changes in optical parameters in terms of structural parameters.

2. Experimental details

BiI_3 was acquired from Sigma Aldrich and utilized exactly as given, with no further purification. Thermal evaporation equipment was used to evaporate BiI_3 thick films of different doses (0, 50, 100, 150, 200, 250, and 300 kG) of γ-radiation (Type E-306A, England). The base pressure was around 10^{-6} Pa., During the evaporation process, a quartz crystal screen (FTM4, Edwards) is outfitted with coating equipment to determine the deposition rate and control the film thickness. The substrate temperature was kept constant at room temperature. To avoid any heating impact during the evaporation of BiI_3, the films were bombarded with 60 °C gamma rays. The source is in Indian groom form 4000/A (available at Atomic Energy Authority, Nasr City, Cairo, Egypt). Average dosage rate from room 1 Gy/s. Dosages have been adjusted to be in the range is (0, 50, 100, 150, 200, 250, and 300 kG). Optical transmittance (T) and reflectance (R) for radioactive films were measured in a normal incident using a double spectroradiometer (UV-vis-NIR JASCO-670). The measurements were performed at room temperature at the wavelength The X-ray diffraction (XRD) pattern range 200 - 2500 nm was obtained using a Philips X-Ray Diffract meter (Model-X'Pert) with Monochromatic Cuk radiation at wavelength = 1.5418.

3. Results and discussion

3.1. XRD analysis

Figure 1 shows XRD patterns with different γ-radiation doses for a BiI_3 thick film with a thickness of 900 nm. The presence of significant peaks in this picture indicates that all of the films analyzed are crystalline. The Rietveld polishing method was used to characterize the examined crystalline material[9]. Figure 1 displays the diffraction peaks of BiI_3 films deposited with different γ-radiation doses in the XRD mode belonging to the rhombic (JCPDS data file: 00-048-1795) structure with the preferred orientation along the (1 1 3) plane. For diffraction angle values 2θ = 12.825, 27, 39.125, 41.645, 46.285, 50.325, 55.765, 58.325 and 63.905 corresponding to (0 0 3), (1 1 3), (1 1 6), (0 0 9), (0 0 3), (1 1 9), (2 2 3)), (2 2 6), (3 0 9) and (2 2 9) planes respectively, and this is in good agreement with the literature[10, 11]. Figure 1 also shows that as the BiI_3 thick films that are treated with γ-radiation pulses the diffraction resistance increases by (1 1 3) levels, revealing the improvement in the crystallization efficiency of the deposited films with the increase of γ-radiation.
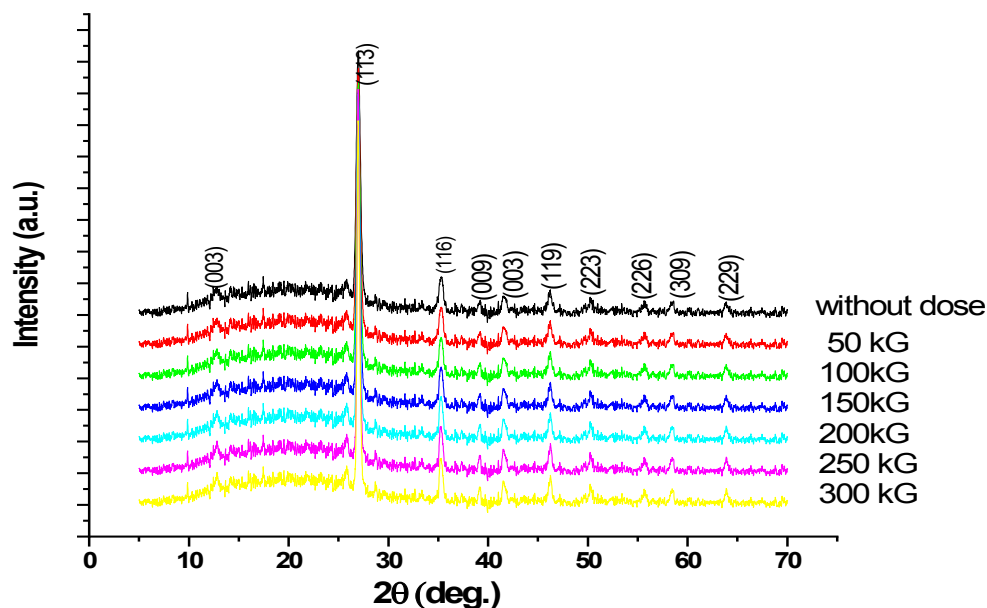
Fig. 1. XRD patterns of BiI₃ with different γ-radiation doses at a thickness of 900 nm.

The instrumentation factor and structure factor, which are ascribed to the crystallite size and lattice strain, are responsible for the peak broadening. Both crystallize size (D) and lattice strain (e) were evaluated using the Scherrer and Wilson equations [12][13]:

$$D = \frac{0.9\lambda}{\beta \cos\theta}$$

(1)

$$e = \frac{\beta}{4\tan\theta}$$

(2)

where β is the structural width that is equivalent to the difference between the sample and the standard (silicon) in the integral X-ray peak profile width and is given as:

$$\beta = \sqrt{\beta_{obs}^2 - \beta_{std}^2} \ .$$

Figure 2 depicts the microstructural characteristics (D and *e*) of BiI₃ films exposed to various γ-radiation doses. With the same film doses, the average crystal size rises from 27 nm to 47 nm, while the lattice strain reduces. Figure 2 compares the microstructure characteristics (D and *e*) of six BiI₃ films with thicknesses varying from 900 nm. The observed behavior of the microchip might be attributed to the larger size of the crystals. This reduction in network strain indicates a reduction in the concentration of network faults.
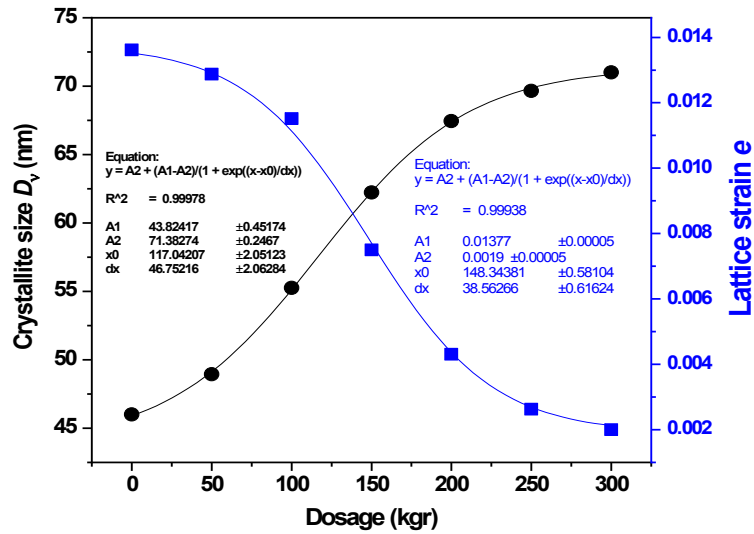
Fig. 2. Variations of the microstructural parameters on BiI$_3$ thick films.

3.2. Effect of g-irradiation on the refractive index (n) and energy gap

The spectrum dependency of the optical transmittance (T) and reflectance (R) of as-deposited and treated films was determined using a double beam spectrophotometer. The fluctuation of the absolute values of T(λ) and R(λ) vs wavelength is seen in Figure 3. The existence of interference fringes and peaks and minima in the transmission spectrum verified the high quality and homogeneity of these BiI$_3$ thick films. Swanepoel's technique was used to calculate the refractive index. This approach comprises recording envelopes centered on the highest interference and the transmission spectrum's minimum [20] [15].
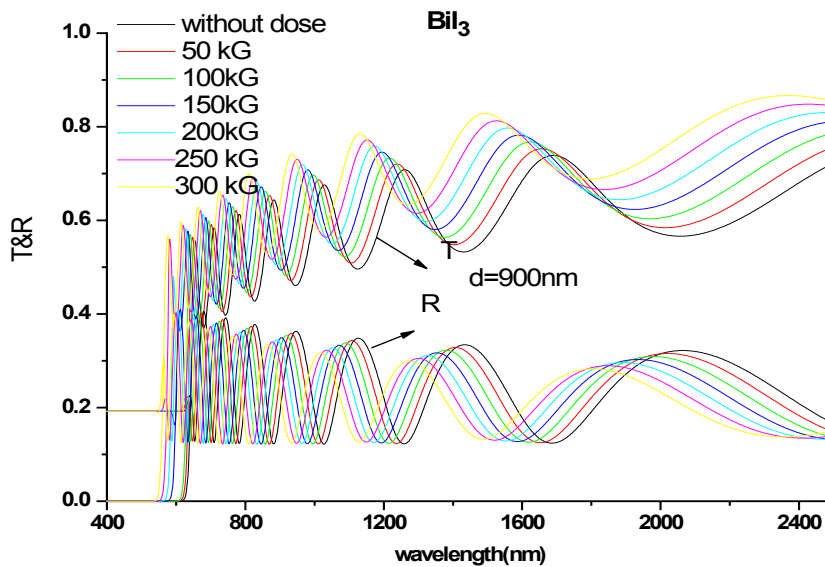
Fig. 3. Transmission and reflection spectra of BiI$_3$ with different γ-radiation doses.

New functions have been introduced to express mathematically the maximum transmission $T_M(\lambda)$ and the minimum transmission/construction envelopes are:

$$T_M\left(\lambda\right)=T_{01}+A_{11}.\exp\left[-\frac{\lambda}{t_{11}}\right]+A_{12}.\exp\left[-\frac{\lambda}{t_{12}}\right]$$

(3)

$$T_m\left(\lambda\right)=T_{02}+A_{21}.\exp\left[-\frac{\lambda}{t_{21}}\right]+A_{22}.\exp\left[-\frac{\lambda}{t_{22}}\right]$$

(4)

The constants values of the two equations namely, (T_{01}, A_{11}, t_{11}, A_{12}, and t_{12}) equation (3) and (T_{02}, A_{21}, t_{21}, A_{22}, and t_{22}) equation (4). According to this method, the refractive index value can be calculated at a given wavelength using the following expression[16][17]:

$$n_j(\lambda)=2.s.\left[\frac{(T_M-T_m)}{(T_M.T_m)}]+\frac{s^2+1}{2}\right]+\sqrt{\{2.s.[\frac{(T_M-T_m)}{(T_M.T_m)}]+[\frac{s^2+1}{2}]\}^2-s^2}$$

(5)

at a given wavelength, T_M and T_m represent the maximum and lowest transmittance. Furthermore, one of these values represents a severe experimental interference, while the other is determined from the equivalent envelope; both envelopes were constructed by computer using the Origin version 7 (Origin Lab Corp.) program and drawn around the extreme of each transmittance spectrum. Furthermore, using the well-known equation, the needed values for the refractive index of the substrate are determined from the spectrum of transmission of the substrate, T_s [18].

$$s=\frac{1}{T_s}+(\frac{1}{T_s}-1)^{\frac{1}{2}}$$

(6)

where $T_s\left(\lambda\right)=[A+B\lambda+C\lambda^2+D\lambda^3]$ and constants A, B, C, and D equal to 0.901414, 8.02369x10^{-5}, 6.13838x10^{-8} and 1.38877x10^{-11}, respectively.

The initial values of the refractive index are deduced and fitted according to the two-term Cauchy dispersion relationship, $n(\lambda)=a+(b/\lambda^2)$ which can be used to extrapolate the complete overall wavelengths[18]

Figure 4 shows the differences in refractive index n as a function of the wavelength of BiI$_3$ thick films with different pulses.
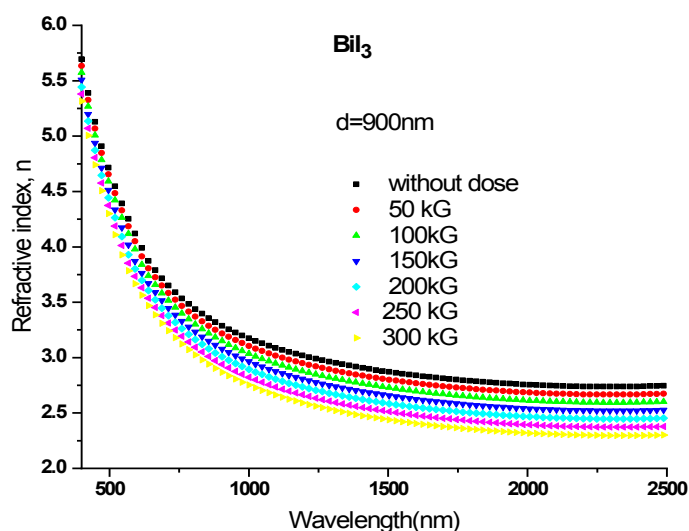
Fig. 4. The spectral dependence of refractive index, n for BiI₃ thick films.

It is seen in Figure 4 that the refractive index decreases with increasing wavelength for all the thick films investigated but also that the refractive index decreases with increasing γ-radiation pulses at all values which can explain the increase in crystal size of these films. Moreover, if n_1 and n_2 have refractive indices at the adjacent maximum (or minimum) at 1 and 2, then the expression gives the film thickness as follows[19]:

$$d_1 = \frac{A}{2} . (\lambda_1 . \lambda_2) \times [\lambda_1 n_2 - \lambda_2 n_1]^{-1} \tag{7}$$

Experimental data for transmittance and reflectivity in the strong absorption area was also used to calculate the optical absorption coefficient using the following relationship [2]:

$$\alpha = \frac{1}{d} \ln \left[\frac{(1-R)^2 + \left[(1-R)^4 + 4R^2 T^2 \right]^{1/2}}{2T} \right] \tag{8}$$

where d is the sample thickness. Figure 5 shows the reliance of the absorption coefficient $\alpha(h\nu)$ on photon energy as a function of film thickness. It is clear in Figure 5 that the fundamental absorption edge related to the optical band gap has higher values greater than 10^5 cm^{-1} for all the investigated films which confirms the ability to use these films in various optoelectronic applications.
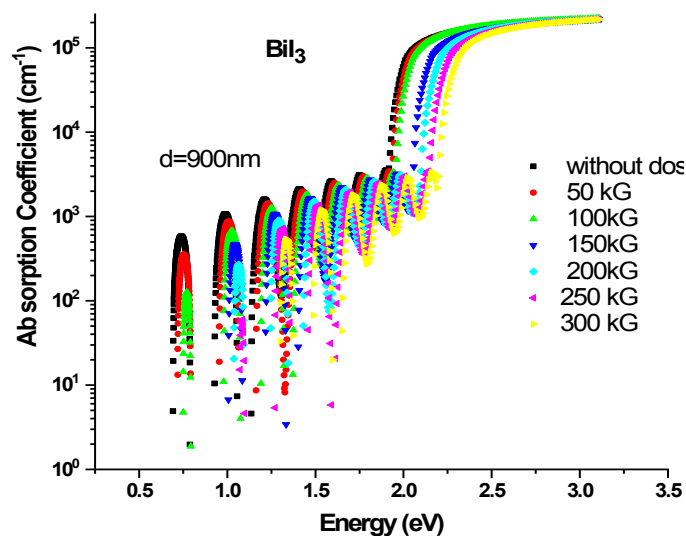
Fig. 5. The dependence of the absorption coefficient on the incident photon energy for BiI$_3$ as-deposited and treated films with γ-radiation doses.

It is known that the absorption coefficient is described in the vicinity of the fundamental absorption edge, for allowing direct band-to-band transitions, neglecting exciton effects as follows[20]:

$$\alpha(h\nu) = \frac{K (h\nu - E_g^{opt})^m}{h\nu} \tag{9}$$

where K is a characteristic (independent of photon energy) parameter for the respective transitions [20], hν denotes photon energy, E_g^{opt} is the optical energy gap, and m is a number that characterizes the transition. $m = 2$ for the majority of amorphous semiconductors (indirect transition) and m = 1/2 for the majority of crystalline semiconductors (direct transition). In the case of nanocrystalline BiI_3 thick film, the direct transition is valid. The absorption coefficient, α (where the absorption is related to interband transitions) can be calculated for higher values ($\alpha \geq 10^4$ cm^{-1}). Figure 6 is a typical best fit of (αhν)^2 vs. photon energy (hν) for BiI_3 films with different γ-radiation doses.
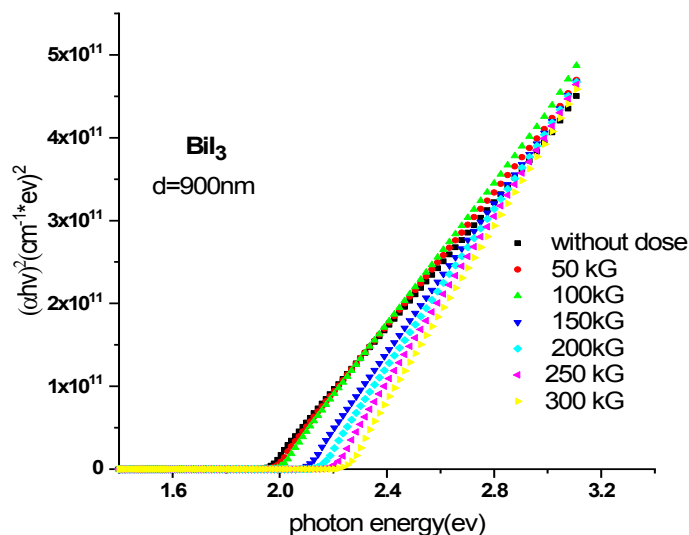
Fig. 6. The plot of (α.hν)^2 versus photon energy, (hν) for BiI$_3$ as-deposited and treated films with γ-radiation doses.

The direct optical band gap E_g^{opt} was taken as the intercept of (α. hν)^2 vs. (hν) at (αhν)^2 = 0 for the allowed direct transition. The determined optical energy gap was about 2.2 eV. Now, we will deal with the so-called second absorption constant, namely the extinction coefficient, ($k_{ex.}$). The values of extinction coefficient, ($k_{ex.}$) have been computed using the following relation [20]

$$k = \alpha\lambda/4\pi \qquad (10)$$

The values of the extinction coefficient, (k_{ex}), of the investigated films, first increase with increasing wavelength until reaching 500 nm, then decrease with increasing wavelength up to 2500 nm, which is related to the increasing probability of absorption processes in the lower wavelength range (Figure 7).
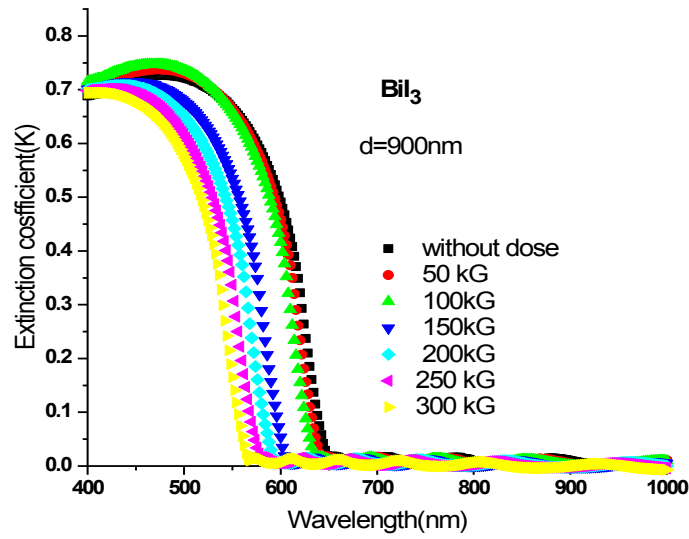
Fig. 7. Variation of extinction coefficient, (k) vs. wavelength, (λ) for BiI₃ as-deposited and treated films with γ-radiation doses.

3.3. Dielectric constant

The dielectric constant is highly reliant on the electronic structure of the material and is directly connected to the density of states inside the forbidden band, which determines the electromagnetic radiation that flows through the material. This feature may be examined using the complex dielectric function, as shown below [20]:

$$\varepsilon = \varepsilon_1 + i\,\varepsilon_2 \tag{11}$$

where 1 denotes the real part of the dielectric constant connection with the process of slowing the light speed in the material 2 is the imaginary component of the dielectric constant that allows dipole movement to absorb energy from the electric field. This also holds for the refractive index and extinction coefficient.

$$\varepsilon_1 = n^2 - k^2 \tag{12}$$

$$\varepsilon_2 = 2nk \tag{13}$$

The differences between ε_1 and ε_2 versus the wavelength are shown in Figure 8 and Figure 9 respectively. It is proved that the dielectric constants decrease with the height of the wavelength while increasing with the increase of the γ-radiation doses on the film, which may be attributed to the increase in the crystal size.
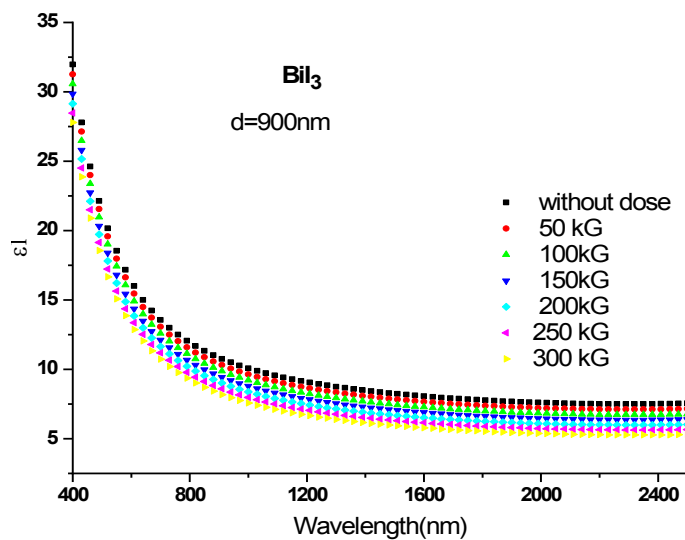
Fig. 8. Variation of real dielectric constant, ε₁ on wavelength, λ for BiI₃ as-deposited and treated films with γ-radiation doses.
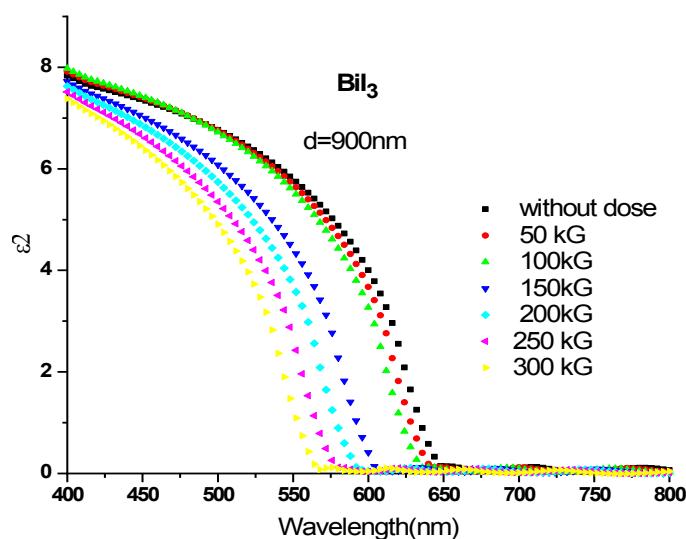
Fig. 9. Variation of imaginary dielectric constant, ε₂ on wavelength, λ for BiI₃ as-deposited and treated films with γ-radiation doses.

3.4. Determination of the optical conductivity

Figure 10 shows the variation of optical conductivity, $\sigma_{opt.}$ as a function of photon energy. The absorption coefficient, α can be used to compute the optical conductivity, $\sigma_{opt.}$ as follows[20]:

$$\sigma_{opt.} = \frac{\alpha n c}{4\pi} \tag{14}$$
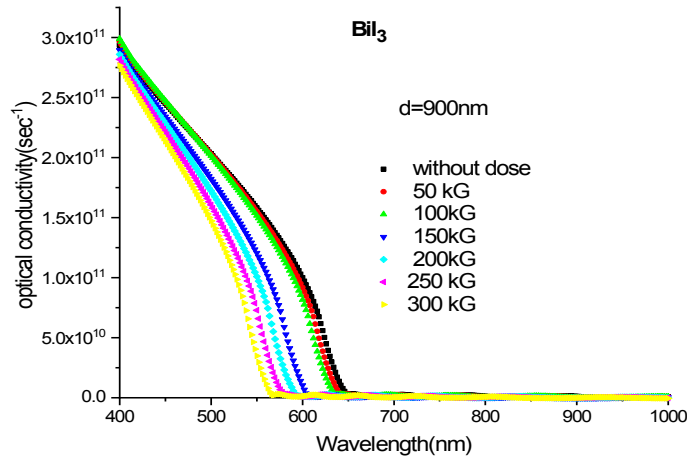
Fig. 10. Dependence of optical conductivity, σ_opt as a function of wavelength λ for BiI₃
as-deposited and treated films with γ-radiation doses.

3.5. Energy loss functions

During the inelastic scattering process in semiconductors, energy is transmitted to or from the uppermost atomic layers. This energy shift implies that electrons are excited both at the surface and at the interface (i.e., in bulk). The spectrum response of this inelastic scattering may be specified using the dielectric theory system as volume energy loss function (VELF) and surface energy loss function (SELF), which are supplied by the following equations[21].

$$VELF = \frac{\varepsilon_2}{\varepsilon_1^2 + \varepsilon_2^2} \tag{15}$$

$$SELF = \frac{\varepsilon_2}{(\varepsilon_1 + 1)^2 + \varepsilon_2^2} \tag{16}$$

Figure 11 and Figure 12 demonstrate the energy dependency of BiI₃ films on the volume and surface energy loss functions, respectively. The graphic shows that the energy loss incurred by free charge carriers when traveling through the volume and the surface are identical. Furthermore, the highest value of the loss functions is close to the absorption edge of the BiI3 films, which is where the interband transition is thought to occur. According to their findings, Al-Mudhaffer et al. [21] found that the maximum value of VELF and SELF falls around the absorption edge of the film.
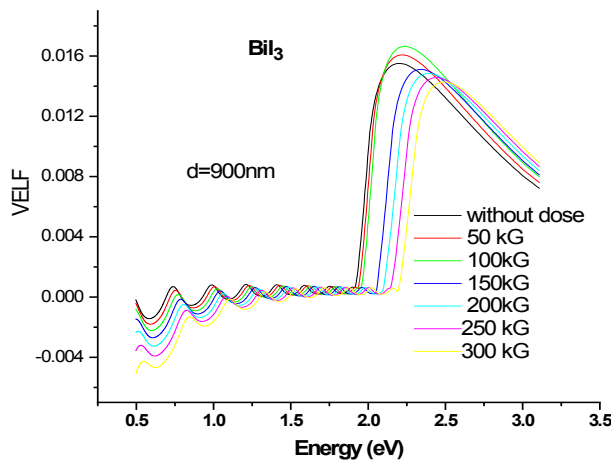
Fig. 11. Dependence of VELF as a function of photon energy, (hv) in the fundamental
absorption region for investigated thick films.
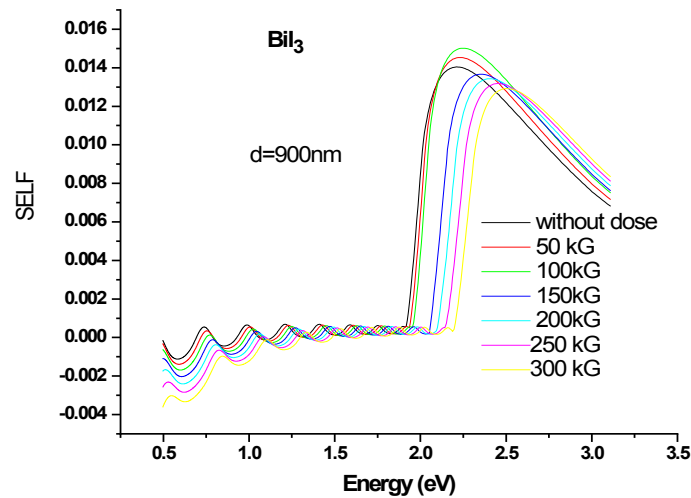
Fig. 12. Dependence of SELF as a function of photon energy, (hν) in the fundamental absorption region for investigated thick films.

3.6. Determination of non-linear refractive index

Non-linear effects occur when high-intensity light propagates across a medium. The incident intensity has a large influence on the non-linear refractive index. When the matter is subjected to a strong electric field from incoming light, polarisation no longer varies proportionally to the electric field, and the change in polarizability must be extended by terms proportional to the square of the electric field [22]. The nonlinear refractive index was deduced in terms of the Tichy and Ticha relationship[23]. Tichy and Ticha relationship is a combination of Miller's popularized rule and static refractive index obtained from the WDD model as[21]:

$$n_2 = [\frac{12\pi}{n_o}]\chi^{(3)} \tag{17}$$

where $\chi^{(3)}$ is third-order non-linear susceptibility. $\chi^{(3)}$ is obtained from the equation[24]

$$\chi^{(3)} = B[\chi^{(1)}]^4 \tag{18}$$

where $\chi^{(1)}$ is linear susceptibility and is given as:

$$\chi^{(1)} = \frac{1}{4\pi}[\frac{E_d}{E_o}] \tag{19}$$

where B= 1.7×10^{-10} (for $\chi^{(3)}$ in esu). $\chi^{(3)}$ is given as:

$$\chi^{(3)} = \frac{B}{(4\pi)^4}\left(n_o^2 - 1\right)^4 \tag{20}$$

Figure 13 and Figure 14 plot the nonlinear refractive index, n_2 versus wavelength, λ. From these figures, we found that the value of the nonlinear refractive index n_2 decreases with increasing wavelength for all BiI_3 thick films while n_2 increases with increasing γ-radiation pulses for the film.
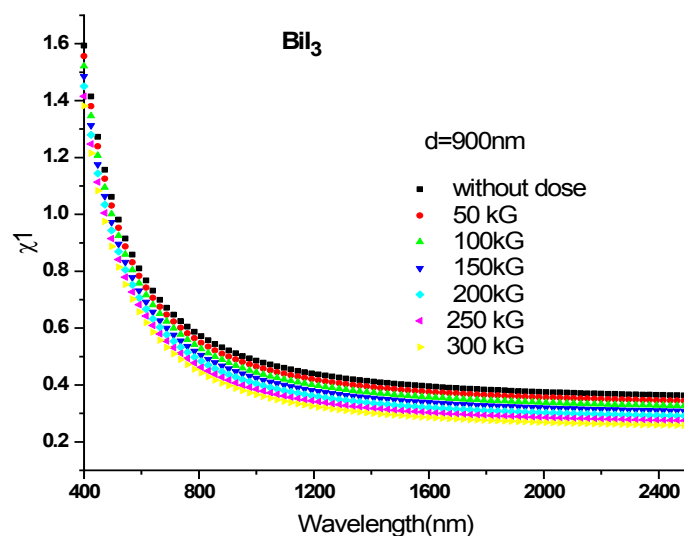
Fig. 13. χ_1 vs wavelength, (λ) for BiI$_3$ as-deposited and treated films with γ-radiation doses.
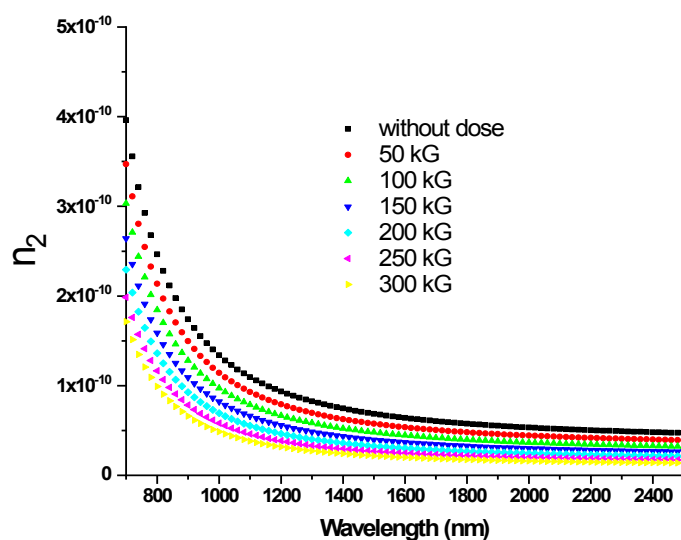
Fig. 14. Dependence of non-linear refractive index, n$_2$ on the wavelength for investigated films.

4. Conclusions

BiI$_3$ thick films with a thickness of 900 nm were successfully synthesized using the thermal evaporation technique. Structural parameters such as crystallite size and microstrain were calculated. The results indicated that the size of the crystals increases while the fine stress decreases with the increase of γ-radiation doses, which indicates the improvement of the crystallization of these films. The effect of γ-radiation doses on the optical properties of BiI$_3$ thick films was studied. The refractive index and thus the extinction coefficient and segregation constants decreased slightly with increasing γ-radiation doses. These slight decreases were explained in terms of increasing crystallite size with increasing γ-radiation doses. The nonlinear refractive index was calculated for the studied samples. The nonlinear refractive index n2 of the studied films is closely related to the linear refractive index n (o). The low optical transmittance and small bandgap of BiI$_3$ films make them a hopeful candidate for optoelectronic devices as well as numerous light detection, modulation, and processing functions.

Acknowledgements

References

[1] E. R. Shaaban, M. A. Osman, A. A. Osman, M. M. Sayed, and K. I. Aly, "Influential role of CdS film thickness in improving CdS/CdTe junction performance for solar cells: structural, optical, and electrical characterizations," J. Mater. Sci. Mater. Electron., vol. 33, no. 7, pp. 4051-4063, 2022; https://doi.org/10.1007/s10854-021-07598-4

[2] M. El-Hagary, M. Emam-Ismail, E. R. Shaaban, and A. El-Taher, "Effect of γ-irradiation exposure on optical properties of chalcogenide glasses Se70S30− xSbx thin films," Radiat. Phys. Chem., vol. 81, no. 10, pp. 1572-1577, 2012; https://doi.org/10.1016/j.radphyschem.2012.05.012

[3] K. S. Shaaban, E. S. Yousef, S. A. Mahmoud, E. A. Wahab, and E. R. Shaaban, "Mechanical, structural and crystallization properties in titanate doped phosphate glasses," J. Inorg. Organomet. Polym. Mater., vol. 30, no. 11, pp. 4655-4663, 2020; https://doi.org/10.1007/s10904-020-01574-x

[4] G. A. Amin, S. M. El-Sayed, H. M. Saad, F. M. Hafez, and M. Abd-El-Rahman, "The radiation effect on optical and morphological properties of Ag-As-Te thin films," Radiat. Meas., vol. 42, no. 3, pp. 400-406, 2007; https://doi.org/10.1016/j.radmeas.2006.12.006

[5] A. F. Abd El-Rehim et al., "Structural and mechanical properties of Lithium bismuth borate glasses containing molybdenum (LBBM) together with their glass-ceramics," J. Inorg. Organomet. Polym. Mater., vol. 31, no. 3, pp. 1057-1065, 2021; https://doi.org/10.1007/s10904-020-01708-1

[6] Z. A. Alrowaili, M. M. Soraya, T. A. Alsultani, A. Qasem, E. R. Shaaban, and M. Ezzeldien, "Sn-induced changes in the structure and optical properties of amorphous As-Se-Sn thin films for optical devices," Appl. Phys. A, vol. 127, no. 2, pp. 1-11, 2021; https://doi.org/10.1007/s00339-020-04175-0

[7] A. S. Jassim, N. A. Dahham, and M. S. Marie, "Study of the Optical Properties for ZnS Thin Film Irradiated by CO2 Laser," Ibn AL-Haitham J. Pure Appl. Sci., vol. 23, no. 3, pp. 58-67, 2017.

[8] E. R. Shaaban, Y. A. M. Ismail, and H. S. Hassan, "Compositional dependence of the optical properties of amorphous Se80− xTe20Bix thin films using transmittance and reflectance measurements," J. Non. Cryst. Solids, vol. 376, pp. 61-67, 2013; https://doi.org/10.1016/j.jnoncrysol.2013.05.024

[9] E. R. Shaaban, "Optical constants and fitted transmittance spectra of varies thickness of polycrystalline ZnSe thin films in terms of spectroscopic ellipsometry," J. Alloys Compd., vol. 563, pp. 274-279, 2013; https://doi.org/10.1016/j.jallcom.2013.02.132

[10] D. Nason and L. Keller, "The growth and crystallography of bismuth tri-iodide crystals grown by vapor transport," J. Cryst. Growth, vol. 156, no. 3, pp. 221-226, 1995; https://doi.org/10.1016/0022-0248(95)00291-X

[11] L. Keller and D. Nason, "Review of X-ray powder diffraction data of rhombohedral bismuth tri-iodide," Powder Diffr., vol. 11, no. 2, pp. 91-96, 1996; https://doi.org/10.1017/S0885715600009040

[12] E. R. Shaaban, I. Kansal, S. H. Mohamed, and J. M. F. Ferreira, "Microstructural parameters and optical constants of ZnTe thin films with various thicknesses," Phys. B Condens. Matter, vol. 404, no. 20, pp. 3571-3576, 2009; https://doi.org/10.1016/j.physb.2009.06.002

[13] J. Zhang et al., "The structural phase transition and mechanism of abnormal temperature dependence of conductivity in ZnTe: Cu polycrystalline thin films," Thin Solid Films, vol. 414, no. 1, pp. 113-118, 2002; https://doi.org/10.1016/S0040-6090(02)00451-0

[14] P. Paufler, "SR Elliott. Physics of amorphous materials. Longman Group Ltd., London, New York, 1984. Pp X+ 386. Price:£ 25.00. ISBN 0-582-44636-8." Wiley Online Library, 1985; https://doi.org/10.1002/crat.2170200922

[15] M. Nowak, "Linear distribution of intensity of radiation reflected from and transmitted through a thin film on a thick substrate," Thin Solid Films, vol. 266, no. 2, pp. 258-262, 1995; https://doi.org/10.1016/0040-6090(96)80030-7

[16] R. Swanepoel, "Determination of the thickness and optical constants of amorphous silicon," J. Phys. E., vol. 16, no. 12, p. 1214, 1983; https://doi.org/10.1088/0022-3735/16/12/023

[17] E. Marquez, J. B. Ramirez-Malo, P. Villares, R. Jimenez-Garay, and R. Swanepoel, "Optical characterization of wedge-shaped thin films of amorphous arsenic trisulphide based only on their shrunk transmission spectra," Thin Solid Films, vol. 254, no. 1-2, pp. 83-91, 1995; https://doi.org/10.1016/0040-6090(94)06267-O

[18] 桑原五郎, "TS Moss: Optical Properties of Semi-conductors, Butterworths scientific Publications, London, 1959, 279 頁, 14× 24cm, 3000 円.," 日本物理学会誌, vol. 14, no. 8, pp. 496-497, 1959.

[19] A. Dahshan, H. H. Amer, and K. A. Aly, "Compositional dependence of the optical constants of amorphous GexAs20Se80− x thin films," J. Phys. D. Appl. Phys., vol. 41, no. 21, p. 215401, 2008; https://doi.org/10.1088/0022-3727/41/21/215401

[20] J. I. Pankove, Optical processes in semiconductors. Courier Corporation, 1975.

[21] M. F. Al-Mudhaffer, M. A. Nattiq, and M. A. Jaber, "Linear optical properties and energy loss function of Novolac: epoxy blend film," Arch. Appl. Sci. Res., vol. 4, no. 4, pp. 1731-7140, 2012.

[22] P. Sharma and S. C. Katyal, "Linear and nonlinear refractive index of As-Se-Ge and Bi doped As-Se-Ge thin films," J. Appl. Phys., vol. 107, no. 11, p. 113527, 2010; https://doi.org/10.1063/1.3428441

[23] H. Ticha and L. Tichy, "Semiempirical relation between non-linear susceptibility (refractive index), linear refractive index and optical gap and its application to amorphous chalcogenides," J. Optoelectron. Adv. Mater, vol. 4, no. 2, pp. 381-386, 2002.

[24] A. Qasem, A. A. Hassan, F. Y. Rajhi, H.-A. S. Abbas, and E. R. Shaaban, "Effective role of cadmium doping in controlling the linear and non-linear optical properties of non-crystalline Cd-Se-S thin films," J. Mater. Sci. Mater. Electron., vol. 33, no. 4, pp. 1953-1965, 2022; https://doi.org/10.1007/s10854-021-07400-5